Propagation of photon-density waves in strongly scattering media containing an absorbing semi-infinite plane bounded by a straight edge

Joshua B. Fishkin and Enrico Gratton

Laboratory for Fluorescence Dynamics, Department of Physics, University of Illinois at Urbana-Champaign, 1110 West Green Street, Urbana, Illinois 61801

Received March 2, 1992; revised manuscript received May 18, 1992; accepted July 2, 1992

Light propagation in strongly scattering media can be described by the diffusion approximation to the Boltzmann transport equation. We have derived analytical expressions based on the diffusion approximation that describe the photon density in a uniform, infinite, strongly scattering medium that contains a sinusoidally intensity-modulated point source of light. These expressions predict that the photon density will propagate outward from the light source as a spherical wave of constant phase velocity with an amplitude that attenuates with distance r from the source as $\exp(-\alpha r)/r$. The properties of the photon-density wave are given in terms of the spectral properties of the scattering medium. We have used the Green's function obtained from the diffusion approximation to the Boltzmann transport equation with a sinusoidally modulated point source to derive analytic expressions describing the diffraction and the reflection of photon-density waves from an absorbing and/or reflecting semi-infinite plane bounded by a straight edge immersed in a strongly scattering medium. The analytic expressions given are in agreement with the results of frequency-domain experiments performed in skim-milk media and with Monte Carlo simulations. These studies provide a basis for the understanding of photon diffusion in strongly scattering media in the presence of absorbing and reflecting objects and allow for a determination of the conditions for obtaining maximum resolution and penetration for applications to optical tomography.

1. INTRODUCTION

Light diffusion in strongly scattering media is of primary importance in several fields, including spectroscopy of highly turbid media and optical imaging of thick tissues.[1–7] After a few scattering events the light propagation process can be treated as a transport of particles that undergo a large number of collisions, performing a random walk through the scattering medium. This diffusion approximation is valid at distances from the light source much larger than the mean free path for light scattering.[8,9] In a macroscopically uniform medium without boundaries the measurement of the average light intensity at different distances from the source and at different angles cannot separate scattering from absorption properties. For the case of multiple scattering of light, fluctuation correlation spectroscopy has been used largely in the study of optical properties, with an emphasis on the determination of the diffusion coefficient of the scattering particles. A large literature on this subject exists, and for a review we refer to Ref. 1. However, when the problem is the identification of macroscopic regions in the scattering medium with different absorption and transport scattering coefficients, this approach cannot be used. In the present approach we neglect the diffusion of the scattering particles. It has been suggested that the use of short light pulses can provide a better approach to the identification of different macroscopic regions with different optical properties, since the time of photon propagation through a strongly scattering medium is related to the effective optical path, which is dependent on the absorption and transport scattering coefficients of the medium. Time gating makes possible discrimination between the direct optical path and the longer photon paths, which permits one to isolate regions of the medium with different optical properties. A number of publications have recently appeared on the different aspects of light pulse propagation and reflection, almost exclusively in the time domain.[4,6,10,11]

In this paper we present the complementary frequency-domain approach, and we show that in the frequency domain the problem of light propagation in strongly scattering media can be treated within the familiar framework of wave phenomena. It must be remembered that, in the frequency-domain method, only the front of the photon-density wave is considered, not the optical light front, which is multiply scattered in the diffusion regime. In particular, we derive the Green's function for the diffusion approximation to the Boltzmann transport equation with a sinusoidally modulated point source, and we experimentally verify the basic predictions of the theory. Having in mind the problem of optical imaging of tissues and its application to medicine, we performed a frequency-domain study of the problem of the diffusion of photons in the presence of a semi-infinite absorbing plane bounded by a straight edge. Our aim in studying the effect of the edge on the diffusing photons is to determine systematically the conditions necessary for obtaining the highest spatial resolution by observing how different parameters of the experiment affect the sharpness of the edge. In this paper we present an analytical solution to the edge problem in the frequency domain that is derived from the above-mentioned Green's function, and we verify with experiments the principal features of the solution. Hebden and Kruger have reported preliminary time-domain ob-

0740-3232/93/010127-14$05.00

servations of the effect of an absorbing edge on photon diffusion.[12] We perform frequency-domain Monte Carlo simulations of particles diffusing in a lattice in which we simulate the presence of an absorbing plane bounded by a straight edge to verify the theoretical prediction further and to compare it with experiments.

The detection of unscattered photons in strongly scattering media has also received attention.[13] Of course, if unscattered light can be detected, optical spectroscopy and optical imaging are feasible in the conventional way. However, for most applications to the medical field, the use of unscattered light for optical imaging is restricted to only a few tissues such as the eye or to tissues that are at most a few millimeters thick.[14]

2. ANALYTICAL SOLUTION FOR A UNIFORM INFINITE MEDIUM

An isotropic source of visible or near-infrared light is immersed in a macroscopically homogeneous, strongly scattering medium. It is assumed for this case that the density of photons $U(\mathbf{r},t)$ and the photon current density $\mathbf{J}(\mathbf{r},t)$ satisfy the diffusion approximation to the Boltzmann transport equation[1,9,15]:

$$\frac{\partial U(\mathbf{r},t)}{\partial t} + v\mu_a U(\mathbf{r},t) + \nabla\cdot\mathbf{J}(\mathbf{r},t) = q_0(\mathbf{r},t), \tag{1a}$$

$$\nabla U(\mathbf{r},t) + \frac{3\partial\mathbf{J}(\mathbf{r},t)}{v^2\partial t} + \frac{\mathbf{J}(\mathbf{r},t)}{vD} = 0, \tag{1b}$$

where v is the speed of a photon in the transporting medium (i.e., water in our experiments), D is the diffusion coefficient, namely,

$$D = \{3[\mu_a + \mu_s(1-g)]\}^{-1}, \tag{2}$$

μ_a is the linear absorption coefficient (i.e., the inverse of the mean free path for photon absorption, with units of inverse distance), μ_s is the linear scattering coefficient (i.e., the inverse of the mean free path for photon scattering), g is the average of the cosine of the scattering angle, and $q_0(\mathbf{r},t)$ is the photon source. Equations (1) imply a tremendous simplification. Use of the diffusion approximation to the Boltzmann transport equation means neglect of interference terms arising from the superpositioning of electromagnetic fields. Polarization as a degree of freedom is also neglected. The density of photons and the photon current density can be accurately calculated from the diffusion approximation to the Boltzmann transport equation when the point of interest is far from sources or boundaries and when the ratio $\mu_s/(\mu_a+\mu_s)$ is close to unity, i.e., when the absorption of the medium is low.[15]

In the case of a sinusoidally intensity-modulated point source of light, the photon source is

$$q_0(\mathbf{r},t) = \delta(\mathbf{r})S\{1 + A\exp[-i(\omega t + \epsilon)]\}, \tag{3}$$

where $\delta(\mathbf{r})$ is a Dirac delta function located at the origin, S is the fluence of the source (in photons per second), A is the modulation of the source, $i = \sqrt{-1}$, ω is the angular modulation frequency of the source, and ϵ is an arbitrary phase. Substituting Eq. (3) into Eq. (1a) and assuming that $U(\mathbf{r},t)$ and $\mathbf{J}(\mathbf{r},t)$ have the forms

$$U(\mathbf{r},t) = [U(\mathbf{r})]_{dc} + [U(\mathbf{r})]_{ac}\exp[-i(\omega t+\epsilon)], \tag{4a}$$

$$\mathbf{J}(\mathbf{r},t) = [\mathbf{J}(\mathbf{r})]_{dc} + [\mathbf{J}(\mathbf{r})]_{ac}\exp[-i(\omega t+\epsilon)], \tag{4b}$$

we obtain the steady-state equations (i.e., the dc part)

$$v\mu_a[U(\mathbf{r})]_{dc} + \nabla\cdot[\mathbf{J}(\mathbf{r})]_{dc} = S\delta(\mathbf{r}), \tag{5a}$$

$$[\mathbf{J}(\mathbf{r})]_{dc} = -vD\nabla[U(\mathbf{r})]_{dc} \tag{5b}$$

and the frequency-dependent equations (i.e., the ac part)

$$(v\mu_a - i\omega)[U(\mathbf{r})]_{ac} + \nabla\cdot[\mathbf{J}(\mathbf{r})]_{ac} = SA\delta(\mathbf{r}), \tag{6a}$$

$$[\mathbf{J}(\mathbf{r})]_{ac} = -vD\left[\frac{1 + i3\omega D/v}{1 + (3\omega D/v)^2}\right]\nabla[U(\mathbf{r})]_{ac}. \tag{6b}$$

We make the assumption that $\omega D \ll v$, which is equivalent to saying that the wavelength in vacuum of the wave of angular frequency ω is much larger than the distance between the scattering particles in the medium. With this assumption Eq. (6b) reduces to

$$[\mathbf{J}(\mathbf{r})]_{ac} \cong -vD\nabla[U(\mathbf{r})]_{ac}. \tag{7}$$

Eliminating the dependent variable $[\mathbf{J}(\mathbf{r})]_{dc}$ from Eqs. (5), we obtain the steady-state diffusion equation

$$\nabla^2[U(\mathbf{r})]_{dc} - (\mu_a/D)[U(\mathbf{r})]_{dc} = -(S/vD)\delta(\mathbf{r}). \tag{8}$$

Eliminating the dependent variable $[\mathbf{J}(\mathbf{r})]_{ac}$ from Eq. (6a) and expression (7), we obtain the frequency-dependent diffusion equation

$$\nabla^2[U(\mathbf{r})]_{ac} - \left(\frac{v\mu_a - i\omega}{vD}\right)[U(\mathbf{r})]_{ac} = -\frac{SA}{vD}\delta(\mathbf{r}). \tag{9}$$

For an infinite medium, Eqs. (8) and (9) can easily be solved to yield

$$\begin{aligned} U(\mathbf{r},t) = {} & \frac{S}{4\pi vDr}\exp\left[-r\left(\frac{\mu_a}{D}\right)^{1/2}\right] + \frac{SA}{4\pi vDr} \\ & \times\exp\left\{-r\left(\frac{v^2{\mu_a}^2+\omega^2}{v^2D^2}\right)^{1/4}\cos\left[\frac{1}{2}\tan^{-1}\left(\frac{\omega}{v\mu_a}\right)\right]\right\} \\ & \times\exp\left\{ir\left(\frac{v^2{\mu_a}^2+\omega^2}{v^2D^2}\right)^{1/4}\sin\left[\frac{1}{2}\tan^{-1}\left(\frac{\omega}{v\mu_a}\right)\right]\right. \\ & \left. - i(\omega t+\epsilon)\right\}. \end{aligned} \tag{10}$$

For a nonabsorbing medium, $\mu_a = 0$, and Eq. (10) reduces to

$$\begin{aligned} U(\mathbf{r},t) = {} & \frac{S}{4\pi vDr} + \frac{SA}{4\pi vDr}\exp\left[-r\left(\frac{\omega}{2vD}\right)^{1/2}\right] \\ & \times\exp\left[ir\left(\frac{\omega}{2vD}\right)^{1/2} - i(\omega t+\epsilon)\right]. \end{aligned} \tag{11}$$

Equation (10) is the Fourier transform equivalent of

$$\rho(\mathbf{r},t) = \frac{1}{(4\pi vDt)^{3/2}}\exp\left(-\frac{r^2}{4vDt} - \mu_a vt\right), \tag{12}$$

which is the time-dependent solution of the diffusion equation as reported by Patterson *et al.*[6] Here, $\rho(\mathbf{r},t)$ is the photon density that satisfies the diffusion approximation to the Boltzmann transport equation when the source term is a narrow pulse given by $q_0(\mathbf{r},t) = \delta(\mathbf{r})\delta(t)$. Examination of Eqs. (10) and (11) shows that the photon density $U(\mathbf{r},t)$ generated by a sinusoidally intensity-modulated point source immersed in a strongly scattering, infinite medium constitutes a scalar field that is propagating at a constant speed in a spherical wave and attenuates as

$\exp(-\alpha r)/r$ as it propagates. Equations (10) and (12) show the practical difference in describing photon diffusion in the frequency domain with respect to its Fourier transform equivalent in the time domain: the photon density generated by a sinusoidally intensity-modulated source at any given modulation frequency propagates with a single phase velocity, while pulses undergo dispersion owing to the different phase velocity of each frequency component of the pulse.

The approach that regards photon transport in strongly scattering media as a diffusional process shows that light emitted from a sinusoidally intensity-modulated point source in such a medium can be treated within the framework of wave phenomena; we therefore refer to $U(\mathbf{r}, t)$ as a photon-density wave. The study of the propagation, the reflection, and the refraction of these waves becomes a trivial problem. For a nonabsorbing medium the photon-density wave emitted from a source of angular modulation frequency ω has a wavelength, from Eq. (11), of

$$\lambda = 2\pi(2vD/\omega)^{1/2}, \tag{13}$$

and its wave front advances at constant speed

$$V = (2vD\omega)^{1/2}. \tag{14}$$

Note that Eqs. (13) and (14), respectively, describe the wavelength and the phase velocity of a photon-density wave, not the wavelength and the phase velocity of the electromagnetic wave, which is multiply scattered for the case of visible and near-infrared light propagating over large distances in strongly scattering media. Sinusoidal modulation of the intensity of a light source in strongly scattering media has the following consequences:

(1) A diffraction pattern caused by an object immersed in a strongly scattering medium should be evident in the presence of a photon-density wave. From the Green's function solution of Eq. (9), we can use the superposition principle to calculate this diffraction pattern caused by the absorbing and/or reflecting object.

(2) An apparent index of refraction of the photon-density wave can be defined as the ratio of the phase velocity of the photon-density wave to the phase velocity of light in vacuum.

(3) The phase velocity is dependent on the modulation frequency of the source but is independent of the distance from the source.

(4) There is an exponential attenuation of the amplitude of a photon-density wave as it propagates in the strongly scattering medium because of the first-order time derivative in Eqs. (1).

Figure 1(a) gives a schematic representation of light intensity measured in response to a narrow pulse emitted into a strongly scattering medium, and Fig. 1(b) shows the time evolution of the intensity measured when light from a sinusoidally intensity-modulated source propagates through the same medium. In Fig. 1(b) the light signal measured by the detector is of the same modulation frequency as that of the light source, but it is shifted in phase and demodulated relative to the light source. The quantities that are measured in a frequency-domain experiment, namely, the phase lag Φ of the signal at the detector relative to the source, the average intensity of the detected signal (i.e., the dc), and the amplitude of the frequency-dependent part of the detected signal (i.e., the ac), are shown in Fig. 1(b). Equation (10) yields expressions for these experimentally determined quantities in a uniform, infinite medium:

$$\Phi = r\left(\frac{v^2\mu_a{}^2 + \omega^2}{v^2D^2}\right)^{1/4} \sin\left[\frac{1}{2}\tan^{-1}\left(\frac{\omega}{v\mu_a}\right)\right], \tag{15}$$

$$\ln[(r)(\mathrm{dc})] = -r\left(\frac{\mu_a}{D}\right)^{1/2} + \ln\left(\frac{S}{4\pi vD}\right), \tag{16}$$

$$\ln[(r)(\mathrm{ac})] = -r\left(\frac{v^2\mu_a{}^2 + \omega^2}{v^2D^2}\right)^{1/4} \times \cos\left[\frac{1}{2}\tan^{-1}\left(\frac{\omega}{v\mu_a}\right)\right] + \ln\left(\frac{SA}{4\pi vD}\right). \tag{17}$$

The above three expressions are linear functions of the source/detector separation r but have a more complicated

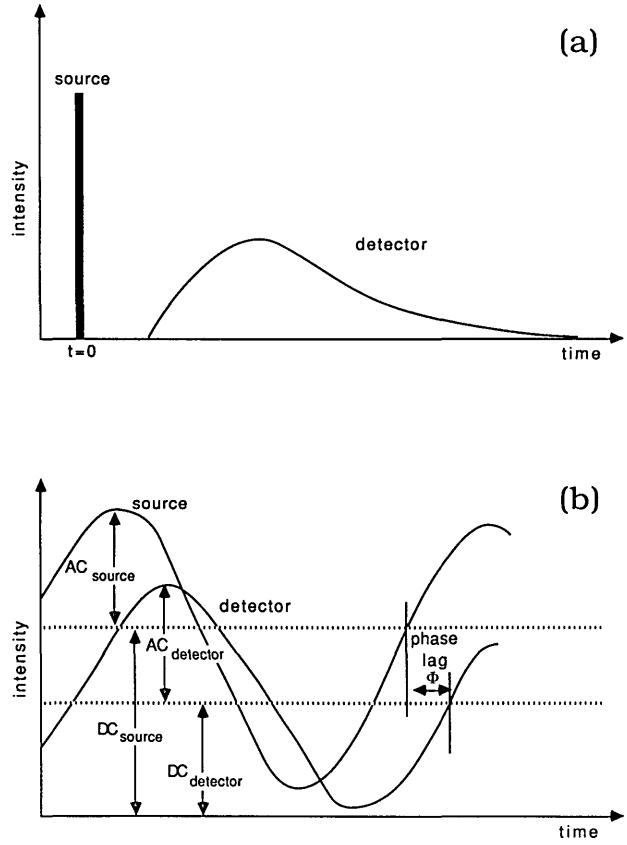

Fig. 1. (a) Schematic representation of the time evolution of the light intensity measured in response to a narrow light pulse traversing an arbitrary distance in a scattering and absorbing medium. If the medium is strongly scattering, there are no unscattered components in the transmitted pulse. (b) Time evolution of the intensity from a sinusoidally intensity-modulated source. The transmitted photon wave retains the same frequency as the incoming wave but is delayed owing to the phase velocity of the wave in the medium. The reduced amplitude of the transmitted wave arises from attenuation related to scattering and absorption processes. The demodulation is the ratio ac/dc normalized to the modulation of the source.

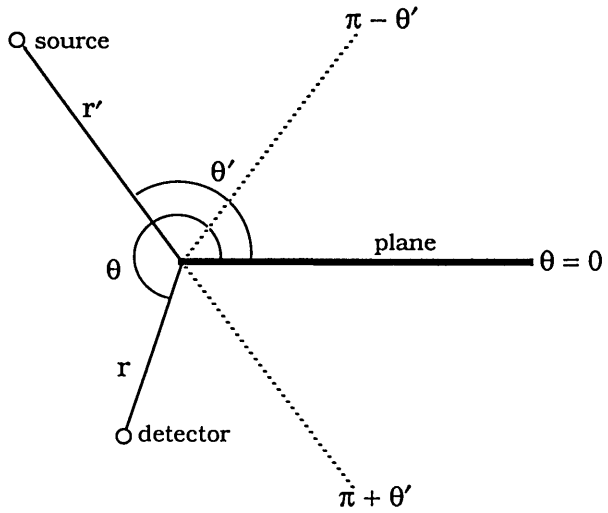

Fig. 2. Cylindrical coordinate system used to describe the configuration of a semi-infinite plane bounded by a straight edge, the point photon source, and the point detector. The edge of the plane lies on the z axis, and the face of the plane is at $\theta = 0$. The coordinates of the point source are (r', θ', z'), and the coordinates of the detector are (r, θ, z).

dependence on ω, v, μ_a, μ_s, and g. Note that the natural logarithm of the demodulation, i.e., ln(ac/dc), is also linear in r. Thus it is seen that the linear dependence on r of Φ, ln[(r)(dc)], and ln[(r)(ac)] is a necessary but not a sufficient condition for the validity of the diffusion approximation to the Boltzmann transport equation. We note that we can obtain the optical properties of a macroscopically homogeneous, infinite, strongly scattering medium by fitting the phase, demodulation, and dc intensity data to Eq. (10) to recover μ_a and D.

3. DIFFRACTION BY AN EDGE

We will now use the Green's functions obtained from Eqs. (8) and (9) above to calculate the diffraction and the reflection of photon-density waves from an absorbing and/or reflecting semi-infinite thin plane bounded by a straight edge, the plane being immersed in an infinite, strongly scattering medium. The study of this problem will provide information about how sharply an edge immersed in a highly turbid medium can appear and what parameters affect the sharpness. In performing the calculation to study the effect of an edge on a photon-density wave, we follow the methodology of Carslaw[16] in his study of a point source of sound in the presence of a thin, rigid semi-infinite plane bounded by a straight edge. Carslaw's research on this topic involves an extension of the methodology developed by Sommerfeld[17] in his study of a single point charge in the presence of an uninsulated, semi-infinite conducting plane at zero potential. So, following Sommerfeld and Carslaw, we use a cylindrical coordinate system with the edge of the semi-infinite plane lying on the z axis and the plane itself at $\theta = 0$. The coordinates of the point source are (r', θ', z'), and the coordinates of the detector are (r, θ, z), as shown in Fig. 2. On inspection of our steady-state and frequency-dependent equations for photon diffusion, i.e., Eqs. (8) and (9), respectively, we see that our physical problem, like the sound-wave problem solved by Carslaw, reduces to the solution of an equation of the form

$$\nabla^2 U + k^2 U = -4\pi\delta(\mathbf{R}) \tag{18}$$

in the twofold Riemann space described by Carslaw,[16] Sommerfeld,[17] and Jeans,[18] where the source/detector separation R is given by

$$R = [r^2 + r'^2 + (z - z')^2 - 2rr'\cos(\theta - \theta')]^{1/2} \tag{19}$$

and where U is a function of r, θ, and z and has the following properties:

(1) It is a finite, single-valued, and continuous function of position in the twofold Riemann space.

(2) It has one and only one infinity, this being at the point (r', θ', z') on the first sheet of the Riemann space, with U approximating the function $\exp(-ikR)/R$ as R approaches zero.

(3) It is zero at $r = \infty$.

Carslaw gives two solutions of Eq. (18) in the twofold Riemann space that satisfy the above conditions[16]:

$$U_1(\theta') = \frac{\exp(-ikR)}{R} - \frac{1}{\pi}\cos\left[\frac{1}{2}(\theta - \theta')\right]\int_0^\infty \frac{\exp\{-ik[r^2 + r'^2 + (z - z')^2 + 2rr'\cosh\beta]^{1/2}\}\cosh(\beta/2)\mathrm{d}\beta}{[r^2 + r'^2 + (z - z')^2 + 2rr'\cosh\beta]^{1/2}[\cos(\theta - \theta') + \cosh\beta]}, \tag{20}$$

$$U_2(\theta') = -\frac{1}{\pi}\cos\left[\frac{1}{2}(\theta - \theta')\right]\int_0^\infty \frac{\exp\{-ik[r^2 + r'^2 + (z - z')^2 + 2rr'\cosh\beta]^{1/2}\}\cosh(\beta/2)\mathrm{d}\beta}{[r^2 + r'^2 + (z - z')^2 + 2rr'\cosh\beta]^{1/2}[\cos(\theta - \theta') + \cosh\beta]}, \tag{21}$$

where $U_1(\theta') = U_2(\theta') = (1/2)\exp(-ikR)/R$ when $\theta = \pi + \theta'$ and $U_1(-\theta') = U_2(-\theta') = (1/2)\exp(-ikR)/R$ when $\theta = \pi - \theta'$. Note that U_1 and U_2 are periodic in θ with a period of 4π. With respect to the dc part of the photon density, we compare Eq. (8), the steady-state diffusion equation, with Eq. (18) and write

$$k_{\mathrm{dc}} \equiv -i(\mu_a/D)^{1/2}, \tag{22}$$

noting that the source strength of Eq. (8) is $-S/vD$ as compared with the source strength of Eq. (18), which is -4π. We then have the two solutions to Eq. (8) in the twofold Riemann space, i.e., $U_{\mathrm{dc1}}(\theta')$ and $U_{\mathrm{dc2}}(\theta')$, these solutions being analogous to $U_1(\theta')$ and $U_2(\theta')$ in Eqs. (20) and (21), respectively, but with the substitution of k_{dc} for k and with an additional pre-exponential factor of $S/4\pi vD$. With respect to the ac part of the photon density, we compare Eq. (9), the frequency-dependent diffusion equation, with Eq. (18) and write

$$k_{\mathrm{ac}} \equiv -i\left(\frac{v\mu_a - i\omega}{vD}\right)^{1/2} \tag{23}$$

or

$$-ik_{\mathrm{ac}} = -\left(\frac{v^2\mu_a^2 + \omega^2}{v^2D^2}\right)^{1/4}\cos\left[\frac{1}{2}\tan^{-1}\left(\frac{\omega}{v\mu_a}\right)\right] + i\left(\frac{v^2\mu_a^2 + \omega^2}{v^2D^2}\right)^{1/4}\sin\left[\frac{1}{2}\tan^{-1}\left(\frac{\omega}{v\mu_a}\right)\right] \tag{24}$$

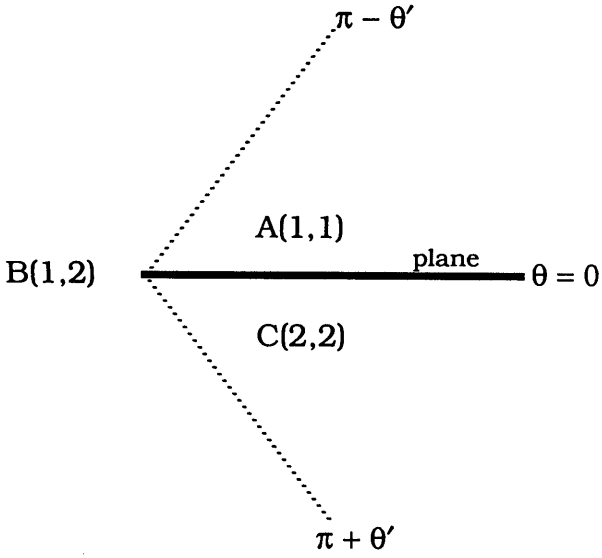

Fig. 3. Division of the physical space into three regions about the semi-infinite plane bounded by a straight edge and the corresponding values of U_1 and U_2 used for $U(\theta')$ and $U(-\theta')$ in each region of the physical space.

and note that the source strength of Eq. (9) is $-SA/vD$. We then have the two solutions to Eq. (9) in the twofold Riemann space, i.e., $U_{ac1}(\theta')$, and $U_{ac2}(\theta')$, which are analogous to $U_1(\theta')$ and $U_2(\theta')$ in Eqs. (20) and (21), respectively, but with the substitution of k_{ac} for k and with an additional pre-exponential factor of $SA/4\pi vD$.

The boundary condition imposed by a semi-infinite absorbing plane is that the photon density U must vanish at $\theta = 0$ and $\theta = 2\pi$. To satisfy this condition, we put poles at (r', θ', z') and $(r', -\theta', z')$ and take the physical space to be the first sheet of the twofold Riemann space, as defined by

$$0 < \theta < 2\pi,$$

and the imaginary space to be the second sheet of the twofold Riemann space, as defined by

$$-2\pi < \theta < 0.$$

Thus

$$\overline{U} = U(\theta') - U(-\theta') \tag{25}$$

satisfies all the conditions of the physical problem posed by an absorbing plane in a strongly scattering medium, where $U(\theta')$ is the source function and $U(-\theta')$ is the image function.

As shown by Carslaw,[16] care must be taken in the choice of proper values for $U(\theta')$ and $U(-\theta')$ in Eq. (25), the choice of these functions being dependent on the value of θ in the physical space. The physical space is divided into three regions, as shown in Fig. 3. In the region $0 \le \theta < \pi - \theta'$ the values for both $U(\theta')$ and $U(-\theta')$ in Eq. (25) are given by U_1. In the region $\pi - \theta' < \theta < \pi + \theta'$, U_1 is taken for $U(\theta')$ and U_2 is taken for $U(-\theta')$. In the region $\pi + \theta' < \theta \le 2\pi$ the values for both $U(\theta')$ and $U(-\theta')$ are given by U_2. At the coordinate $\theta = \pi - \theta'$, U_1 is taken for $U(\theta')$ and $(1/2)\exp(-ikR)/R$ is taken for $U(-\theta')$, where R is defined in Eq. (19) as the source/detector separation. At the coordinate $\theta = \pi + \theta'$, $(1/2)\exp(-ikR)/R$ is taken for $U(\theta')$ and U_2 is taken for $U(-\theta')$. Thus the solution to the problem of the absorbing semi-infinite plane takes the following forms (refer to Fig. 3):

Region A:

$$\overline{U}_{dc} = U_{dc1}(\theta') - U_{dc1}(-\theta'), \tag{26}$$

$$\overline{U}_{ac} = U_{ac1}(\theta') - U_{ac1}(-\theta'); \tag{27}$$

Region B:

$$\overline{U}_{dc} = U_{dc1}(\theta') - U_{dc2}(-\theta'), \tag{28}$$

$$\overline{U}_{ac} = U_{ac1}(\theta') - U_{ac2}(-\theta'); \tag{29}$$

Region C:

$$\overline{U}_{dc} = U_{dc2}(\theta') - U_{dc2}(-\theta'), \tag{30}$$

$$\overline{U}_{ac} = U_{ac2}(\theta') - U_{ac2}(-\theta'); \tag{31}$$

At $\pi - \theta'$:

$$\overline{U}_{dc} = U_{dc1}(\theta') - \frac{1}{2}\frac{S}{4\pi vD}\frac{\exp[-R(\mu_a/D)^{1/2}]}{R}, \tag{32}$$

$$\overline{U}_{ac} = U_{ac1}(\theta') - \frac{1}{2}\frac{SA}{4\pi vD}\frac{\exp(-ik_{ac}R)}{R}; \tag{33}$$

At $\pi + \theta'$:

$$\overline{U}_{dc} = \frac{1}{2}\frac{S}{4\pi vD}\frac{\exp[-R(\mu_a/D)^{1/2}]}{R} - U_{dc2}(-\theta'), \tag{34}$$

$$\overline{U}_{ac} = \frac{1}{2}\frac{SA}{4\pi vD}\frac{\exp(-ik_{ac}R))}{R} - U_{ac2}(-\theta'). \tag{35}$$

We see from Eqs. (26) and (27) that at $\theta = 0$, $\overline{U}_{dc} = 0$ and $\overline{U}_{ac} = 0$ for $0 < r < \infty$, and from Eqs. (30) and (31) we see that at $\theta = 2\pi$, $\overline{U}_{dc} = 0$ and $\overline{U}_{ac} = 0$ for $0 < r < \infty$.

For a reflecting semi-infinite plane the boundary condition is that $(1/r)\partial U/\partial\theta$ must vanish at $\theta = 0$ and $\theta = 2\pi$. This condition is met in a manner that is analogous to the solution for the photon-absorbing plane, the only difference being that for the reflecting plane we add the source function to the image function to satisfy the boundary condition.

Thus

$$\overline{U} = U(\theta') + U(-\theta') \tag{36}$$

satisfies the boundary condition imposed by a reflecting plane in a strongly scattering medium.

For the case of a semi-infinite plane that has a probability p_{abs} of absorbing a photon that collides with it, the solution of the physical problem is given by

$$\overline{U} = U(\theta') - p_{abs}U(-\theta') + (1 - p_{abs})U(-\theta'). \tag{37}$$

When $p_{abs} = 1$, Eq. (37) reduces to Eq. (25), the solution for the absorbing plane, and when $p_{abs} = 0$, Eq. (37) reduces to Eq. (36), the solution for the reflecting plane. If some of the light is able to pass through the plane, we add an isotropic source term such as Eq. (10) above at point (r', θ', z') with a coefficient proportional to the transmission probability and we normalize the absorption, reflection, and transmission probabilities.

The phase shift Φ relative to the source, the average (dc) intensity, and the amplitude of the frequency-dependent part of the signal (the ac) are given by

$$\Phi = \tan^{-1}\left[\frac{\mathrm{Im}(\overline{U}_{ac})}{\mathrm{Re}(\overline{U}_{ac})}\right], \tag{38}$$

$$\mathrm{dc} = \overline{U}_{dc}, \tag{39}$$

$$\mathrm{ac} = [\mathrm{Re}(\overline{U}_{ac})^2 + \mathrm{Im}(\overline{U}_{ac})^2]^{1/2}, \tag{40}$$

respectively, and

$$\text{demodulation} = \mathrm{ac}/\mathrm{dc}, \tag{41}$$

where $\mathrm{Re}(\overline{U}_{ac})$ and $\mathrm{Im}(\overline{U}_{ac})$ are, respectively, the real and the imaginary parts of $\overline{U}_{ac}$.

4. MONTE CARLO SIMULATION

To confirm further the validity of the analytical solution and to treat problems with more complicated boundary conditions, we implemented a Monte Carlo simulation program to trace individual photon histories. We simulated a point source of photons in a homogeneous cubic lattice in which each cell has a probability for absorption and scattering. We also added a semi-infinite absorbing plane bounded by a straight edge to the homogeneous lattice, where the plane had the thickness of a lattice cell. We performed the simulations by using a random-number generator to sample discrete events from probability distributions derived from the speed of a photon, v, in the scattering medium, the absorption coefficient μ_a, the scattering coefficient μ_s, and the average cosine of scattering angle, g. In a given simulation we built up a time histogram in the three-dimensional lattice by tracing at least 10^6 individual photon histories. We then performed a fast Fourier transform on the time histogram at each point in the lattice to obtain a frequency-domain Monte Carlo simulation, that is, a simulation of an intensity-modulated point source in a strongly scattering medium. The size of the lattice was such that, for the value of μ_a used, no photon escaped the lattice.

5. EXPERIMENTAL APPARATUS AND METHOD

We have studied the photon-transport properties of strongly scattering media through frequency-domain experiments on 3.78 L of skim milk mixed with quantities of black India ink varying from no ink to 2000 μL of ink. We have qualitatively compared the data from the analytical solutions, the Monte Carlo simulations, and the skim-milk experiments.

For the skim-milk experiments our light source was a Spectra Diode Laboratories SDL-2431-H2 diode laser with a 1-m fiber optic pigtail of diameter 100 μm. The average diode current was set at values ranging from 200 to 830 mA and was sinusoidally modulated with a Marconi Instruments Model 2022A signal generator with its output amplified by a Model M502C wideband rf amplifier from RF Power Labs, Inc. In a given experiment, light was transferred from the diode laser into the skim-milk/black-India-ink medium through the optical fiber pigtail of the diode laser, the end of the fiber being immersed in the milk/black-ink solution. The wavelength of the diode-laser light was 810 nm, and the intensity of the light source was modulated at frequencies ranging from 20 to 120 MHz, the modulation frequency being fixed for a given experiment. The light detector was a 3-mm-diameter optical fiber bundle with one end immersed in the skim-milk solution and the other end attached to a Hamamatsu R928 photomultiplier. The photomultiplier signals were processed by a cross-correlation electronics system using the digital acquisition system described by Feddersen *et al.*[19] In the course of the skim-milk experiments, care was taken to keep the ends of the source and detector optical fibers as far as possible from the walls of the solution container and from the surface of the solution. The entire setup was completely protected from room light that could influence the dc measurement.

Three types of experiment were performed by the Monte Carlo simulations and the skim-milk/black-India-ink experiments. In one type of experiment we measured the phase shift Φ, the dc intensity, and the ac amplitude of the light intensity [Fig. 1(b) above] at a given modulation frequency as a function of the source/detector separation r to verify the validity of the diffusion approximation result of Eq. (10) above. Here, the phase data were recorded relative to the phase measurement made at the shortest source/detector separation distance, and the dc and ac data were normalized to the respective dc and ac values made at the shortest source/detector separation distance. In the case in which this experiment was performed on skim milk, the end of the detector optical fiber was immersed in the milk at a distance r from the source optical fiber, with the ends of the two fibers pointing in the same direction, as shown in Fig. 4. This orientation of the end of the detector fiber relative to the end of the source optical fiber ensured that only scattered photons were detected. In the skim-milk experiments the source/detector separation was varied from 2.5 to 9.6 cm in increments of 0.115 cm during the course of an experiment. The two other types of experiment were undertaken to verify the validity of Eqs. (26)–(35) above. We measured the effect that an absorbing semi-infinite plane immersed in our scattering media had on the intensity-modulated light. The geometry for these experiments is explained in the caption to Fig. 5. We measured the phase shift Φ, the dc

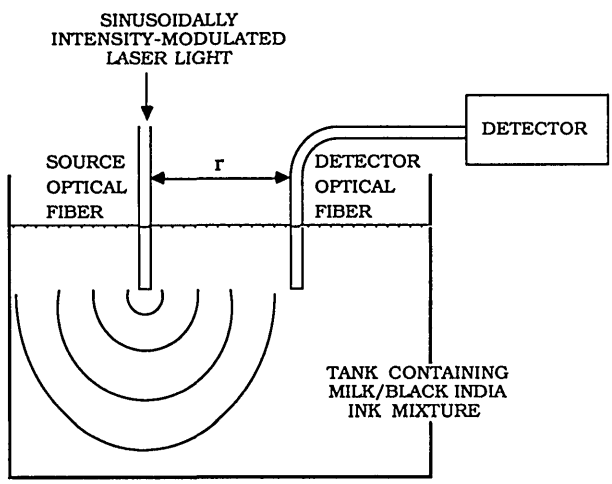

Fig. 4. Schematic of the experimental setup used to test the validity of the diffusion approximation result of Eq. (10) above.

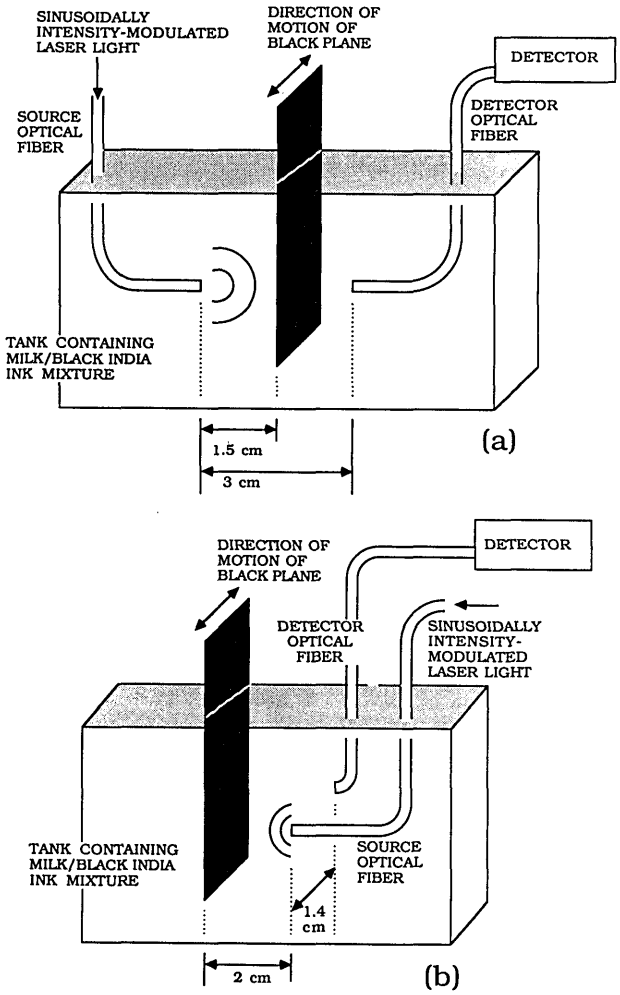

Fig. 5. (a) Setup for a diffraction measurement: the ends of the source and detector optical fibers are set a fixed distance apart (3 cm) on opposite sides of the absorbing plane, the face of the absorbing plane is oriented perpendicularly to the line joining the ends of the source and detector optical fibers, and each point of the face of the plane is equidistant from the end of each optical fiber. Measurements are performed as a function of the position of the edge of the plane relative to the line joining the source and the detector optical fibers. The 0-cm position of the plane edge is defined to be the point where the edge of the plane crosses the line joining the ends of the source and detector optical fibers. (b) Setup for a reflection measurement: same as that in (a), except that now the ends of the source and detector optical fibers are set a fixed distance (1.4 cm) apart on the same side of the absorbing plane, with the ends of the optical fibers pointing in a direction that is perpendicular to the face of the plane. The 0-cm position of the plane edge is defined to be the point where the edge of the plane crosses the line coming from the end of the source optical fiber.

intensity, the ac amplitude, and the demodulation of the signal at a given modulation frequency for each position of the source and detector optical fibers relative to the edge of the plane. The phase data were recorded relative to the phase measurement made when the source and the detector were in their initial positions relative to the edge of the plane, that is, where the plane was far from the source and the detector and the dc intensity, ac amplitude, and demodulation data, respectively, were normalized to the dc intensity, ac amplitude, and demodulation values recorded for the initial position of the source and the detector relative to the edge of the plane.

6. RESULTS OF EXPERIMENTS ON HOMOGENEOUS MEDIA

Figures 6–9 show plots derived from frequency-domain experiments in homogeneous mixtures of skim milk and black India ink and from frequency-domain Monte Carlo simulations. Figure 6 shows the phase shift of the detected sinusoidally intensity-modulated light signal versus the source/detector separation in media of different absorptions μ_a. The linearity of the phase shifts in Fig. 6 with respect to the source/detector separation r is consistent with the predictions of Eq. (15) above, indicating that the photon density generated by a sinusoidally intensity-modulated light source propagates with a single phase velocity through the strongly scattering media. Figure 7 shows phase-shift values at four source/detector separations versus the square root of the modulation frequency of the light intensity. Equation (15) predicts that for $\mu_a = 0$ the phase will increase linearly as the square root of the modulation frequency, which is not the case for the data shown in Fig. 7, owing to μ_a's being equal to 0.000125/mm

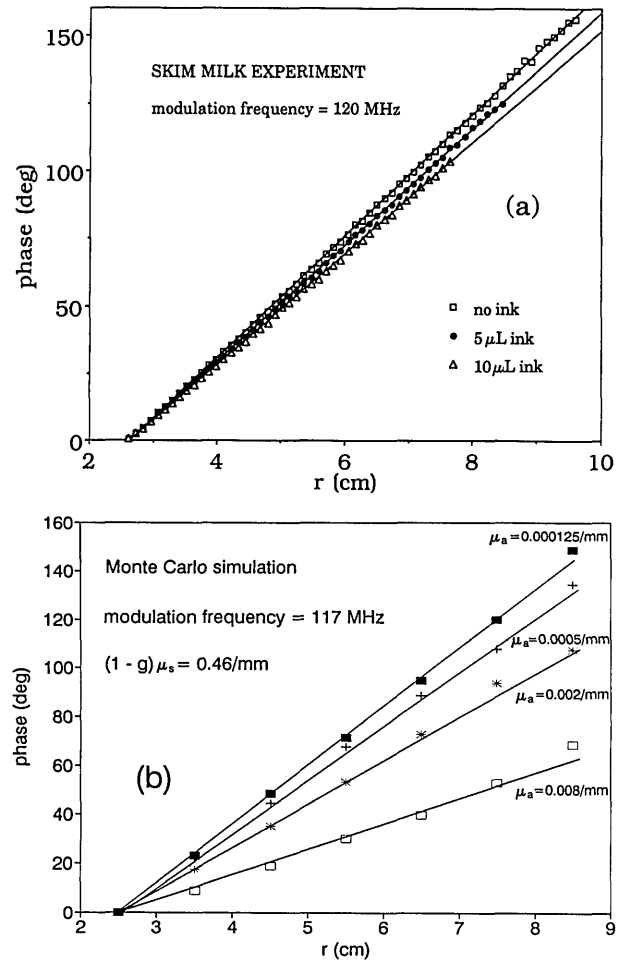

Fig. 6. Phase lag versus source/detector separation r, where the source and the detector are immersed in 3.78 L of skim milk mixed with three amounts of black India ink. The phase data were plotted relative to the phase measured with the shortest source/detector separation. The data were collected at a 120-MHz modulation frequency. The correlation coefficients for the lines fitting data of each milk/ink mixture are equal to 1.000. (b) Frequency-domain Monte Carlo simulation of phase lag versus source/detector separation r for four values of μ_a. The data were plotted relative to the phase at 2.5 cm from the source.

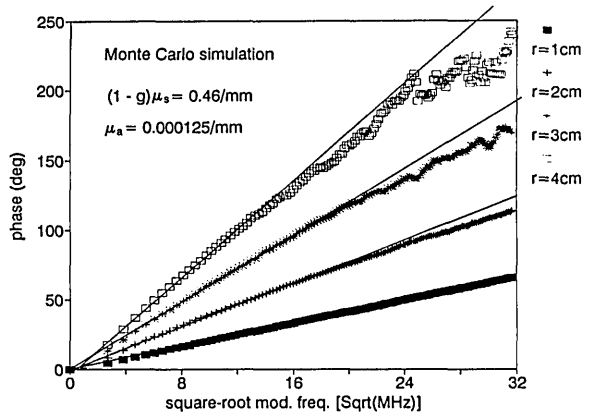

Fig. 7. Frequency-domain Monte Carlo simulation of phase lag versus the square root of modulation frequency. Each set of data was obtained at a fixed source/detector separation.

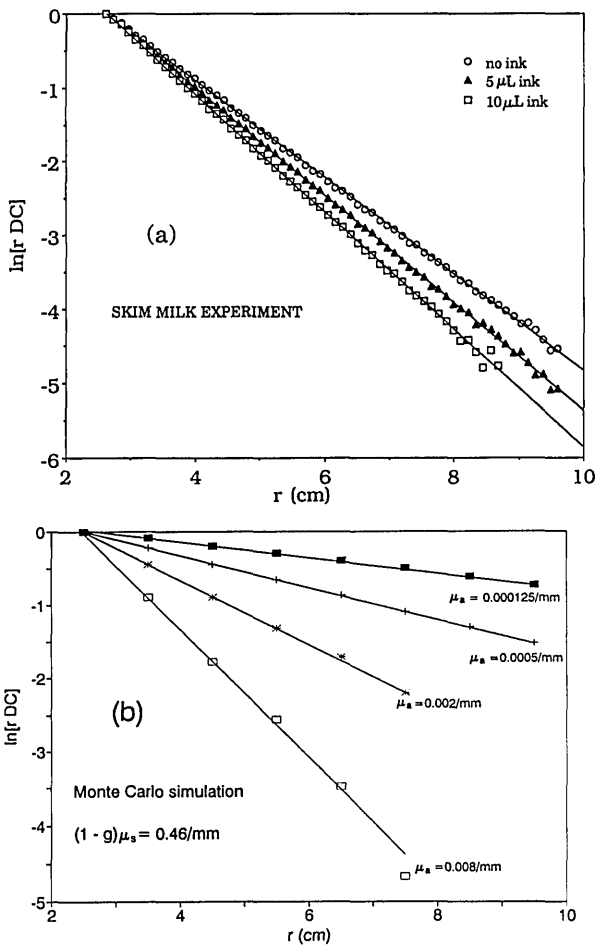

Fig. 8. (a) Natural logarithm of the source/detector separation r multiplying the dc intensity obtained at r, versus r, where the source and the detector are immersed in 3.78 L of skim milk mixed with three amounts of black India ink. The data are normalized to the r dc value at r = 2.5 cm. The correlation coefficients for the lines fitting these data are equal to 1.000. (b) Monte Carlo simulation of ln(r dc) versus r for four values of μ_a. The data are normalized to the r dc value at r = 2.5 cm.

in this particular frequency-domain Monte Carlo simulation. Figures 8 and 9 report plots of the natural logarithm of the source/detector separation r multiplying the dc intensity and the ac intensity of the detected light signal versus the source/detector separation r in media of different absorptions μ_a. The linearity of the fits to the data in Figs. 8 and 9 is consistent with the predictions of Eqs. (16) and (17) respectively, as are the decreasing values of the slopes of the linear fits to the data in Figs. 8 and 9 with respect to the increasing media absorption μ_a.

The slopes of the linear fits to the phase-shift data of Fig. 6(a) were used in the calculation (Table 1) of values for the wavelength λ and the phase velocity V of sinusoidally intensity-modulated light at 120-MHz modulation frequency as it propagates in the homogeneous scattering medium (3.78 L of skim milk mixed with no ink to 10 μL of black India ink). Comparing the wavelength and the phase velocity of the 120-MHz light-intensity wave in a vacuum with the wavelength and the phase velocity of the 120-MHz photon-density wave in the skim-milk media,

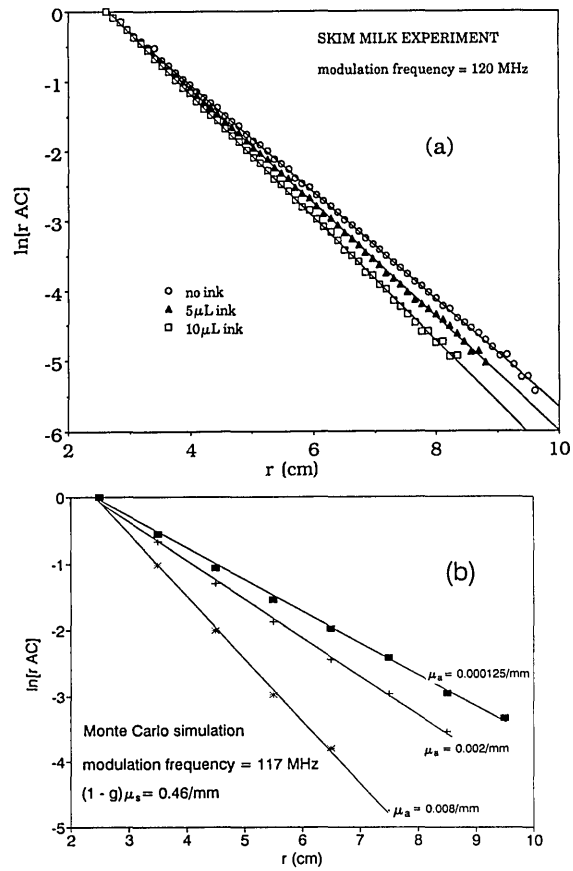

Fig. 9. (a) Natural logarithm of the source/detector separation r multiplying the ac amplitude obtained at r, versus r, where the source and the detector are immersed in 3.78 L of skim milk mixed with three amounts of black India ink. The data are normalized to the r ac value at r = 2.5 cm. The correlation coefficients for the lines fitting these data are equal to 1.000. (b) Frequency-domain Monte Carlo simulation of ln(r ac) versus r for three values of μ_a. The data are normalized to the r ac value at r = 2.5 cm.

Table 1. Wavelength and Phase Velocity of a Photon Density Wave in 3.78 L of Skim Milk Mixed with Black India Ink[a]

	λ (mm)	V (mm/s)
No ink	160	1.92×10^{10}
5 μL of black ink	168	2.02×10^{10}
10 μL of black ink	176	2.11×10^{10}

[a] $\omega/2\pi$ = 120 MHz.

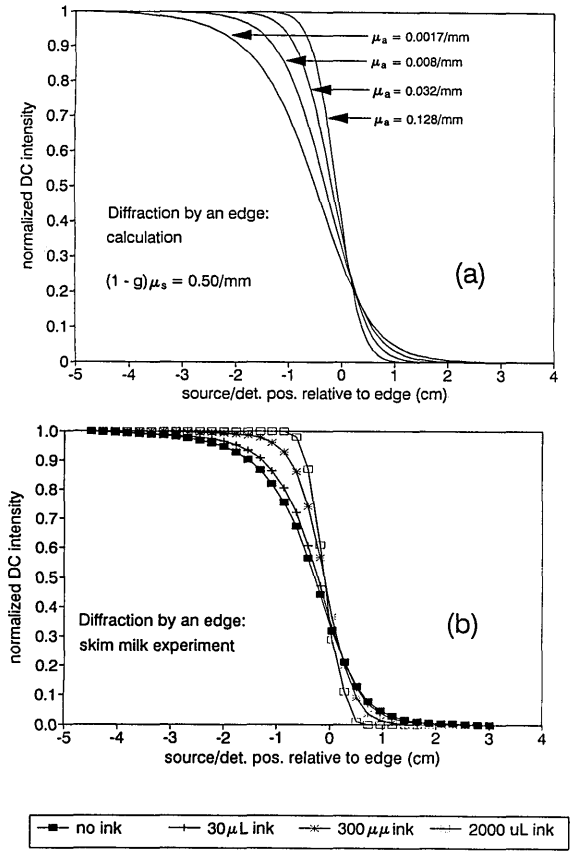

Fig. 10. (a) Plots calculated from diffusion theory of dc intensity at four medium absorptions versus the position of an absorbing edge. (b) Measurement in skim milk mixed with four amounts of black India ink of dc light intensity versus the position of an absorbing edge.

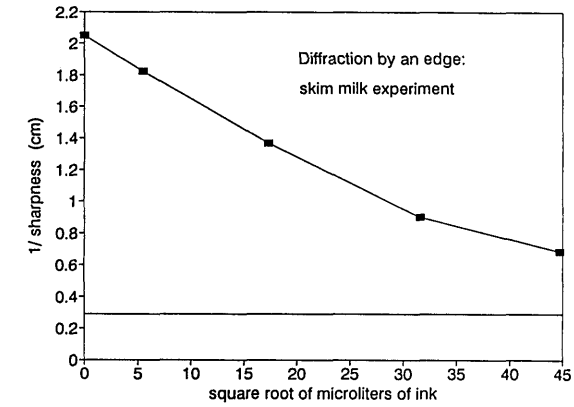

Fig. 11. Inverse sharpness of an edge (the sharpness is the inverse of the distance moved by the edge, relative to the source/detector position, that causes the intensity to decrease from 90% to 10% of the initial value) versus the square root of the volume of black India ink in the skim milk. This figure was derived from the plots in Fig. 10(b).

we see that the wavlength and the phase velocity of the photon-density wave in skim milk are reduced by a factor of the order of 10 relative to the wavelength and the phase velocity, respectively, of the light-intensity wave in a vacuum. The values in Table 1 show that, as the medium absorption increases, the wavelength of the photon-density wave increases, as does the phase velocity. The magnitude of the photon-absorbing properties of a transporting medium thus has implications for the use of sinusoidally intensity-modulated light in the imaging of objects immersed in strongly scattering media: the effect of increasing the photon-absorbing properties of a scattering medium reduces the resolving power of the frequency-dependent part of the photon density by increasing its wavelength. This result is consistent with Eq. (10) above. Note that Eq. (10) also predicts that increasing the density of scatterers in a transporting medium improves the resolving power of the frequency-dependent part of the photon density by reducing its wavelength. As the results in Section 7 will show, the ability to resolve an object immersed in a highly scattering medium may be improved by

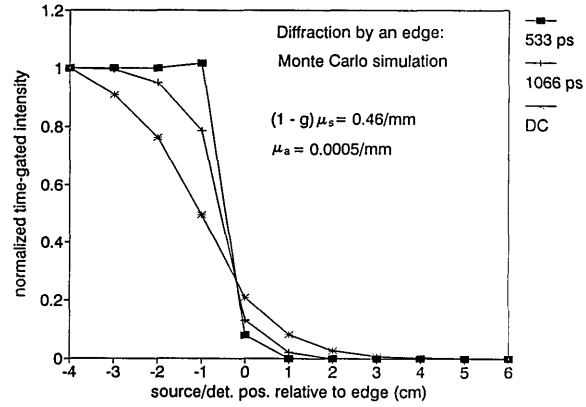

Fig. 12. Monte Carlo simulation of the time-gated intensity versus the position of an absorbing edge.

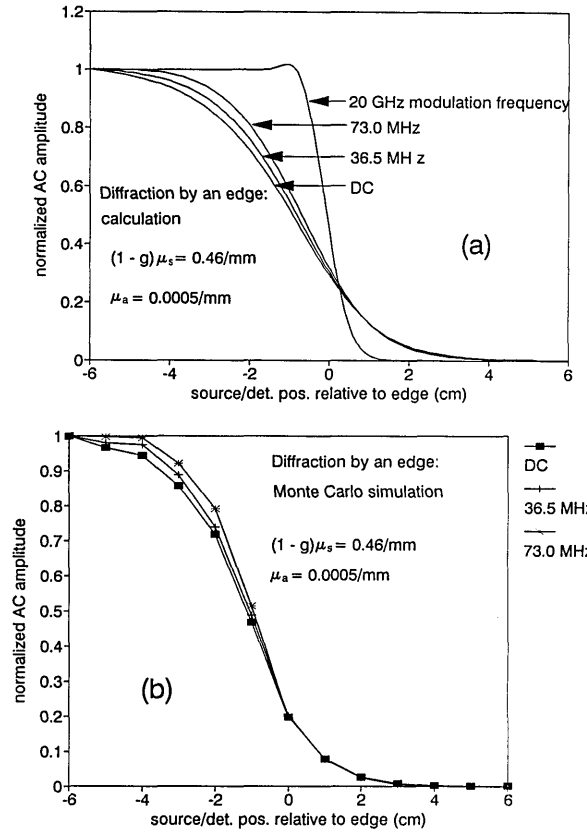

Fig. 13. (a) Plots calculated from diffusion theory of ac amplitude at four modulation frequencies versus the position of an absorbing edge. (b) Frequency-domain Monte Carlo simulation of ac amplitude at three modulation frequencies versus the position of an absorbing edge.

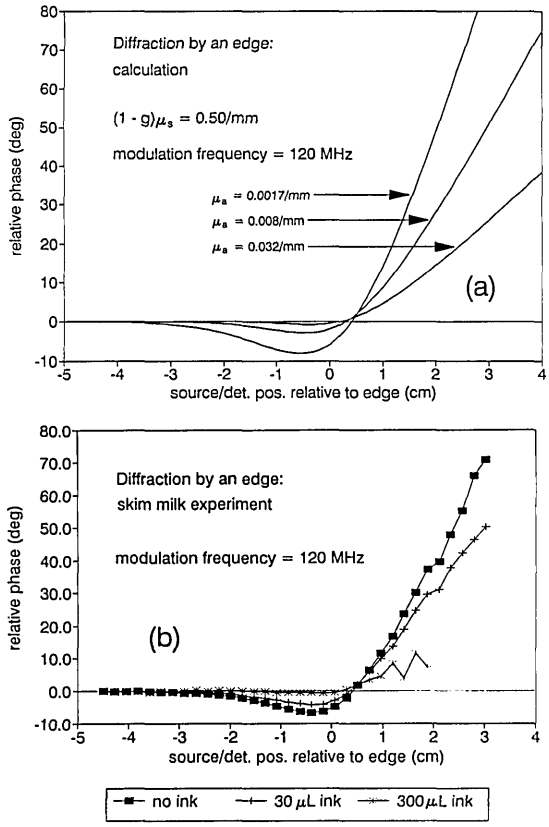

Fig. 14. (a) Plots calculated from diffusion theory of the relative phase at three media absorptions versus the position of an absorbing edge. (b) Measurement in skim milk mixed with three amounts of black India ink of the relative phase versus the position of an absorbing edge.

an increase in the photon-absorption properties of the medium if properties of the dc part (instead of the ac part) of the photon density are used in the imaging process.

7. DIFFRACTION AND REFLECTION BY AN ABSORBING EDGE: SIMULATIONS AND EXPERIMENTS

Figures 10–19 were obtained with the use of the geometry shown in Fig. 5(a) above. Figure 10 shows plots of the normalized dc light intensity of a diffracted signal in scattering media of different absorptions versus the source/detector position relative to an absorbing edge. The plots of Fig. 10(a) are derived from diffusion theory, and the plots of Fig. 10(b) were obtained from the detection of the dc light intensity in skim milk mixed with different amounts of black India ink. The sharpness in the decrease in dc intensity in Fig. 10 increases with increasing photon absorption in the medium, owing to the deletion of photons traveling relatively long path lengths from the source to the detector. We define the sharpness as the inverse of the distance moved by the edge, relative to the source/detector line, that causes a decrease in the intensity from 90% to 10% of its initial value. Increasing absorption leads to a narrowing of the distribution of photon paths from the source to the detector, resulting in a sharpening of the intensity decrease as the edge of the plane cuts into the narrowing bundle of light. Figure 11 shows a plot of inverse sharpness of the decrease in dc intensity versus the square root of the volume of black India ink mixed with skim milk. Note that the inverse sharpness plotted in Fig. 11 appears asymptotically to approach 0.3 cm, which is the diameter of the aperture of the detector optical fiber. Figure 10 shows that when the edge is exactly between the source and the detector, the dc light intensity is less than one half of the maximum. This is a consequence of the diffusion of the photons, which allows for the deletion of photon paths that would have crossed the area occupied by the edge multiple times. Figure 12 shows a Monte Carlo simulation of the normalized time-gated light intensity versus the source/detector position relative to an absorbing edge in a diffraction experiment. The sharpness of the time-gated intensity plot in Fig. 12 increases with the separation of the earlier photons from the rest of the photons, which is a consequence of the earlier photons' traversing a relatively straight path in their movement from the source to the detector (i.e., the earlier photons undergo relatively few collisions). Figure 13 shows plots derived from diffusion theory and from a frequency-domain Monte Carlo simulation of the normalized ac amplitude of the photon density generated by a source that is sinusoidally modulated at different modulation frequencies versus the source/detector position relative to an absorbing edge in a diffraction experiment. The sharpness of the normalized ac amplitude in Fig. 13 increases with increasing modulation frequency. At high modulation frequencies, only those photons traveling a relatively straight path from the source to the detector

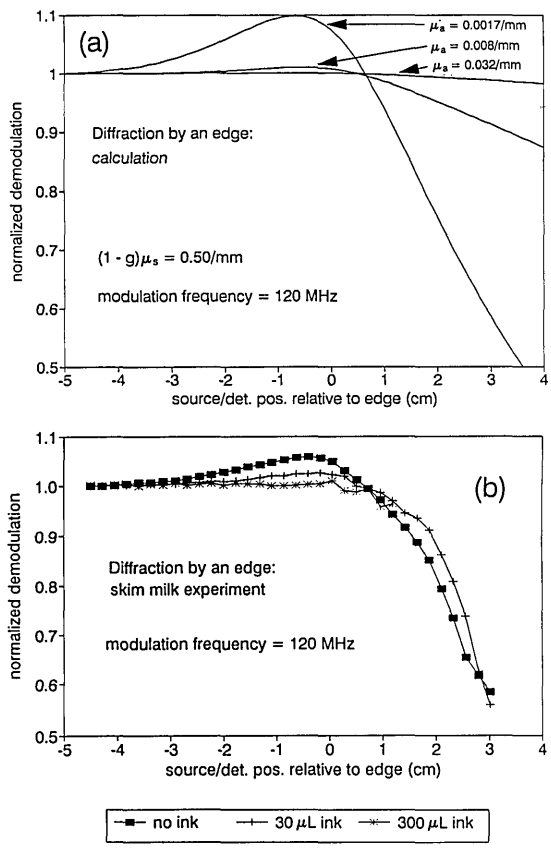

Fig. 15. (a) Plots calculated from diffusion theory of the demodulation at three media absorptions versus the position of an absorbing edge. (b) Measurement in skim milk mixed with three amounts of black India ink of signal demodulation versus the position of an absorbing edge.

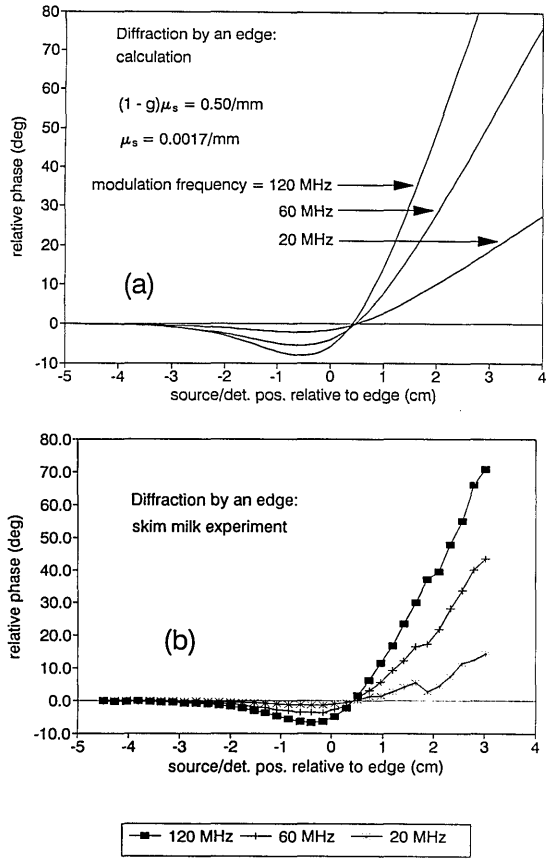

Fig. 16. (a) Plots calculated from diffusion theory of the relative phase at three modulation frequencies versus the position of an absorbing edge. (b) Measurement in skim milk of the relative phase at three modulation frequencies versus the position of an absorbing edge.

survive, owing to the $\exp(-\alpha r)/r$ attenuation of the ac part of the signal. In comparing the plots of Fig. 10 with the plots of Figs. 12 and 13, we can see that the photon-absorption properties of a medium and the time resolution of the scattered photons are analogous insofar as how they affect the resolution of the absorbing edge in the scattering medium. Higher photon absorption in the medium provides sharper resolution of the edge when the dc intensity of the light signal is measured, owing to the deletion from the medium of photons traveling relatively longer path lengths from the source to the detector; faster time gating or higher modulation frequencies provide sharper resolution of the edge in measurements of the time-gated or frequency-dependent part of the signal, owing to the detection of photons undergoing relatively few scattering events. Figures 14 and 15, respectively, show plots of the phase and the demodulation of a diffracted signal at 120-MHz modulation frequency versus the source/detector position relative to an absorbing edge in media of different absorptions. The plots of Figs. 14(a) and 15(a) are derived from diffusion theory, and the plots of Figs. 14(b) and 15(b) were obtained from the detection of a sinusoidally intensity-modulated light signal in skim milk mixed with different amounts of black India ink. Figures 16 and 17, respectively, show plots of the phase and the demodulation of a diffracted signal at different modulation frequencies versus the source/detector position relative to an absorbing edge. The plots of Figs. 16(a) and 17(a) are derived from diffusion theory, and the plots of Figs. 16(b) and 17(b) were obtained from the detection of a sinusoidally intensity-modulated light signal in skim milk. Figures 18 and 19, respectively, show plots of the phase and the demodulation of a diffracted signal at different modulation frequencies versus the source/detector position relative to an absorbing edge. The plots of Figs. 18(a) and 19(a) are derived from diffusion theory, and the plots of Figs. 18(b) and 19(b) are from a frequency-domain Monte Carlo simulation.

The frequency-resolved plots of Figs. 14–19 show that the phase first decreases as the source and the detector approach the zero position and then sharply increases. The overall magnitude of the effect decreases as the photon absorption within the medium increases. To explain this effect qualitatively, we must consider that at the detector we are measuring the contribution of photons traveling throughout a distribution of paths. As the source and the detector approach the zero position, the field of view becomes occupied by the absorbing edge, and all the longer paths that would have crossed the boundary now occupied by the edge are deleted. This deletion causes an effective advance of the average wave front and an increase in the modulation of the signal. As the source and the detector move closer to the zero position, the phase reaches its minimum value and the modulation reaches its maximum value. When the edge passes the zero position, all the shorter paths are deleted, and the wave front is strongly retarded and demodulated. The addition of ink effectively deletes the longer photon paths, thereby de-

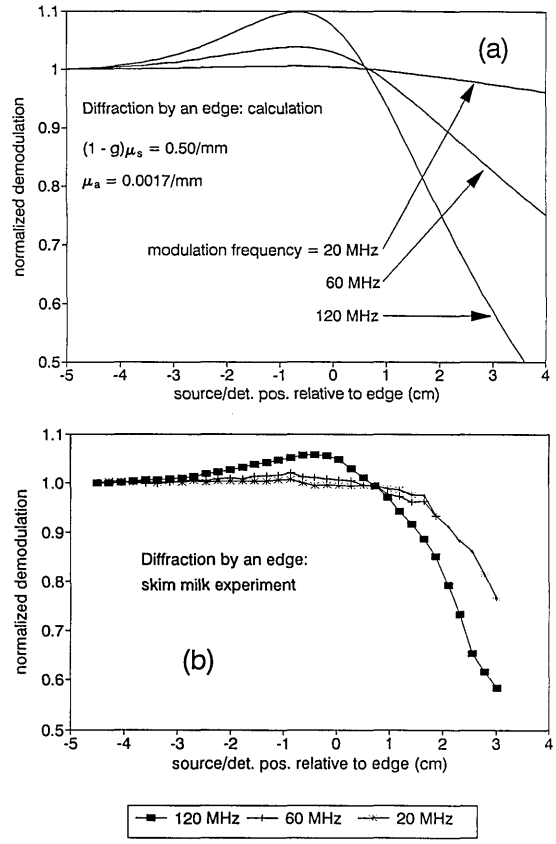

Fig. 17. (a) Plots calculated from diffusion theory of the demodulation at three modulation frequencies versus the position of an absorbing edge. (b) Measurement in skim milk of the signal demodulation at three modulation frequencies versus the position of an absorbing edge.

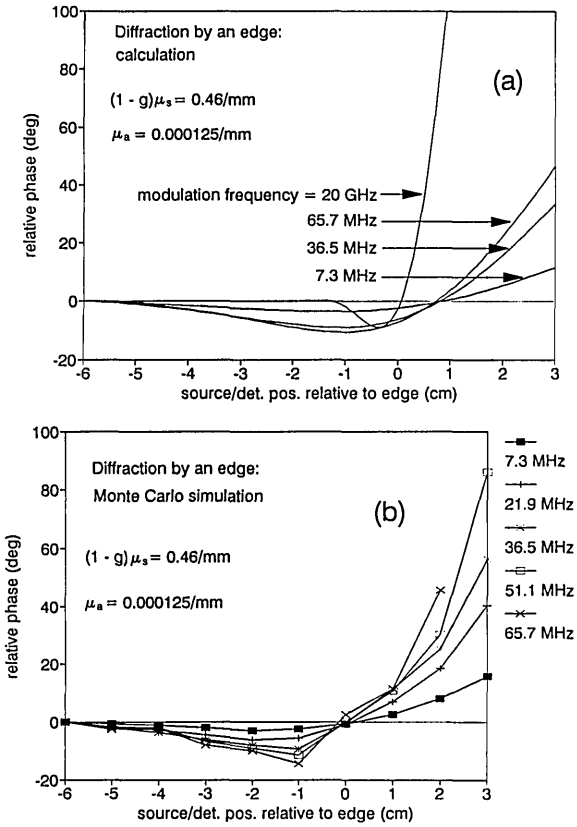

Fig. 18. (a) Plots calculated from diffusion theory of the relative phase at four modulation frequencies versus the position of an absorbing edge. (b) Frequency-domain Monte Carlo simulation of the relative phase at five modulation frequencies versus the position of an absorbing edge.

creasing the overall effect. In the limit of high absorption the phase difference caused by the insertion of the edge becomes small since the effective wave velocity is high.

Figures 20 and 21, respectively, show plots of the phase and the demodulation of a reflected signal at different modulation frequencies versus the source position relative to an absorbing edge. These plots were acquired with the use of the geometry shown in Fig. 5(b) above. The plots of Figs. 20(a) and 21(a) are derived from diffusion theory, and the plots of Figs. 20(b) and 21(b) were obtained from the detection of a sinusoidally intensity-modulated light signal in skim milk. The plots of Figs. 20 and 21 show that the phase decreases as the source approaches the zero position and then reaches a constant value, while the modulation increases and then reaches a constant value. The qualitative explanation of this effect is almost identical to the qualitative explanation of the behavior of the phase and the demodulation in the diffraction experiment, the only difference being that the phase and the modulation reach a constant value in the reflection experiment because the source and the detector are on the same side of the plane; when the edge of the plane passes the source and the detector, the distribution of the photon paths between the source and the detector becomes constant.

8. CONCLUSION

The diffusion approximation to the Boltzmann transport equation fully describes our experiments of propagation of photons in macroscopically homogeneous infinite media for all the absorptions investigated. The range of absorption and transport scattering coefficients that we have studied is typical of many animal tissues in the near-infrared region.[6] At high absorption or at distances from the light source that are of the order of the mean free path for light scattering, the diffusion approximation should fail.[15] Given the value of $(1 - g)\mu_s$ and the value of μ_a for light of 810-nm wavelength in skim milk, which we determined from our data to be 0.50/mm and 0.0017/mm, respectively, few unscattered photons will survive the transit from the source to the detector when the source/detector separation is of the order of a few centimeters. (Note that for our measurements the minimum source/detector separation was 2.5 cm.) However, at short distances from the source, unscattered photons will contribute to the light intensity. We have performed other experiments, not reported here, in which we have studied the angular dependence of the light intensity in a milk suspension. We have oriented the end of the detector optical fiber either directly toward the source or away from the source, and we have measured the same intensity in the medium within errors. Only when the detector was very close to the source, less than a centimeter for the skim-milk experiment, did we observe a definitive dependence of the light intensity on the orientation of the end of the detector optical fiber relative to the source. The effects on the measured light intensity in the milk suspension that are due to the boundary of the tank containing

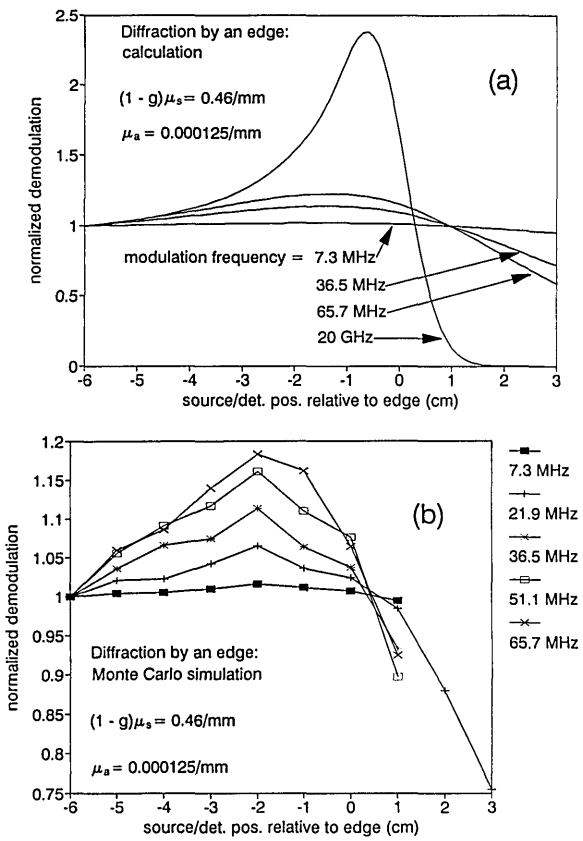

Fig. 19. (a) Plots calculated from diffusion theory of the demodulation at four modulation frequencies versus the position of an absorbing edge. (b) Frequency-domain Monte Carlo simulation of the demodulation at five modulation frequencies versus the position of an absorbing edge.

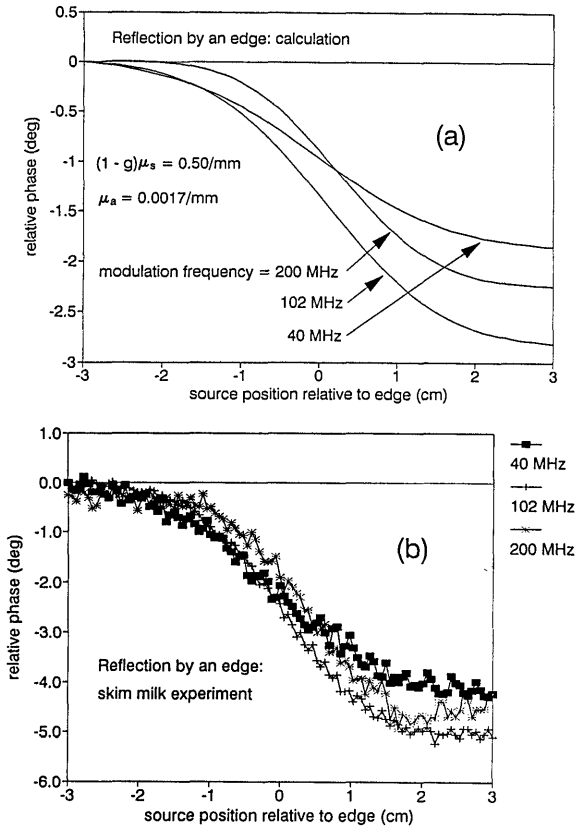

Fig. 20. (a) Plots calculated from diffusion theory of the relative phase at three modulation frequencies versus the position of an absorbing edge. (b) Measurement in skim milk of the relative phase at three modulation frequencies versus the position of an absorbing edge. The light source that was used to generate these data was a synchronously pumped Rhodamine 6G single-jet dye laser that was cavity dumped at 2 MHz. The dye laser was tuned to a wavelength of 690 nm. Apart from the light source, the experimental setup is as described in Section 5.

the milk suspension were also studied; deviations from the expected behavior (based on the diffusion approximation for an infinite medium) were observed, these were due to the light exchange with the room rather than to the presence of the boundaries. The milk suspension acts as a condenser for light, since the photon density is inversely proportional to the photon diffusion coefficient. An optical fiber immersed in the milk suspension measures a higher photon intensity than that measured by the fiber in the room (assuming isotropic illumination).

For the purpose of spectroscopy and the imaging of thick tissues, the scattered light component provides the only contribution of the light transmitted through the sample, since the unscattered component is already strongly attenuated at distances comparable with the mean free path. The amount of the scattered component that is transmitted depends only on the absorption of the sample. To put this scattered component to better use, we superimpose a sinusoidal amplitude modulation upon the intensity of the light source, or we can pulse the light source. The photon-density wave reproduces some of the features of the original electromagnetic wave of wavelength λ and allows for the recovery of the spectroscopic parameters $\mu_a(\lambda)$ and $[1 - g(\lambda)]\mu_s(\lambda)$ from a measurement of the ac phasor. [As was noted by Patterson *et al.*, a limitation of the model based on the diffusion approximation is the ambiguity between g and μ_s, since only the product $(1 - g)\mu_s$ can be obtained.[6]] However, since the propagation is by diffusion, the amplitude-modulated term attenuates as $\exp(-\alpha r)/r$ as the photon-density wave advances (even with no photon absorption). Consequently the amplitude-modulated term, which carries information on the optical parameters, becomes negligible after propagation through 10–15 cm of scattering medium (with properties similar to those of tissues) at rf modulation. To obtain good spatial resolution, one must increase the amplitude modulation frequency, which also reduces the penetration of the photon-density wave at that modulation frequency. As a consequence of the $\exp(-\alpha r)/r$ attenuation of the ac amplitude, there is a quasi-linear relationship between the wavelength of the photon-density wave and the penetration of the photon-density wave in a strongly scattering medium when $\mu_a = 0$. Given the exponential nature of the attenuation process, there is only a logarithmic advantage in increasing the source intensity.

The edge resolution experiments show that the basic rule that governs the resolution or the sharpness of the edge is the deletion of the longer photon paths. Several processes and measurement protocols can cause the effective deletion of the longer path: photon absorption, high modulation frequency, and faster time gating. The mechanism by which the sharpness of an edge is increased

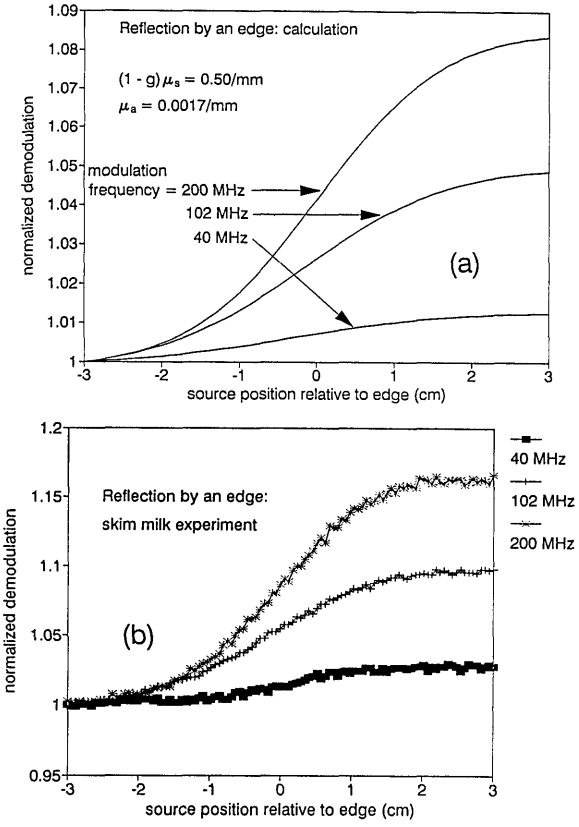

Fig. 21. (a) Plots calculated from diffusion theory of the demodulation at three modulation frequencies versus the position of an absorbing edge. (b) Measurement in skim milk of the signal demodulation at three modulation frequencies versus the position of an absorbing edge. The light source described in the caption to Fig. 20(b) was used in the acquisition of these data, but, apart from the light source, the experimental setup is as described in Section 5.

can easily be explained from the perspective of a bundle of photon paths that join the source to the detector. The thinner the light bundle, the closer the approach to the computer tomography geometry. In practice, the effective light bundle can be made very narrow, of the order of a millimeter for source/detector distances of 3–5 cm and absorption and scattering transport coefficients of the order of those found in animal tissues in the near infrared. The ultimate resolution or sharpness of an edge should not be confused with the detectability of a small object. The detectability is determined by the precision of the phase and demodulation measurement, which can be extremely high.[20] Instead, the sharpness of an edge or the separation of two small objects depends on the optical properties of the medium, modulation frequency, or time gating. Since we have obtained the analytical solution for some typical cases, we understand how the optical properties and modulation frequency or time gating determine the sharpness of an edge.

The measurement of the photon-density wave front provides a simple and powerful method to detect macroscopic inhomogeneities in a scattering medium. An absorbing object causes a wave-front deformation that is easy to measure. We are studying the limit of resolvability of small absorbing objects in highly turbid media.

ACKNOWLEDGMENTS

These experiments and analyses of the data produced were performed at the Laboratory for Fluorescence Dynamics (LFD) in the Department of Physics at the University of Illinois at Urbana-Champaign (UIUC). The LFD and this study are supported jointly by the Division of Research Resources of the National Institutes of Health (RR03155) and UIUC. The authors thank Julie Butzow for help in preparing this paper.

REFERENCES

1. A. Ishimaru, *Wave Propagation and Scattering in Random Media* (Academic, New York, 1978).
2. M. J. Stephen, "Temporal fluctuations in wave propagation in random media," Phys. Rev. B **37,** 1–5 (1988).
3. R. Berkovits and S. Feng, "Theory of speckle-pattern tomography in multiple-scattering media," Phys. Rev. Lett. **65,** 3120–3123 (1990).
4. B. White, P. Sheng, M. Postel, and G. Papanicolaou, "Probing through cloudiness: theory of statistical inversion for multiply scattered data," Phys. Rev. Lett. **63,** 2228–2231 (1989).
5. J. R. Singer, F. A. Grunbaum, P. Kohn, and J. P. Zubelli, "Image reconstruction of the interior of bodies that diffuse radiation," Science **248,** 990–993 (1990).
6. M. S. Patterson, B. Chance, and B. C. Wilson, "Time resolved reflectance and transmittance for the non-invasive measurement of tissue optical properties," Appl. Opt. **28,** 2331–2336 (1989).
7. D. J. Pine, D. A. Weitz, P. M. Chaikin, and E. Herbolzheimer, "Diffusing-wave spectroscopy," Phys. Rev. Lett. **60,** 1134–1137 (1988).
8. P. W. Anderson, "The question of classical localization: a theory of white paint?" Philos. Mag. B **52,** 505–509 (1985).
9. A. Ishimaru, "Diffusion of light in turbid material," Appl. Opt. **28,** 2210–2215 (1989).
10. B. Chance, S. Nioka, J. Kent, K. McCully, M. Fountain, R. Greenfeld, and G. Holtom, "Time-resolved spectroscopy of hemoglobin and myoglobin in resting and ischemic muscle," Anal. Biochem. **174,** 698–707 (1988).
11. B. White, P. Sheng, Z. Q. Zhang, and G. Papanicolaou, "Wave localization characteristics in the time domain," Phys. Rev. Lett. **59,** 1918–1921 (1987).
12. J. C. Hebden and R. A. Kruger, "A time-of-flight breast imaging system: spatial resolution performance," in *Time-Resolved Spectroscopy and Imaging of Tissues,* B. Chance, ed., Proc. Soc. Photo-Opt. Instrum. Eng. **1431,** 225–231 (1991).
13. K. M. Yoo, F. Liu, and R. R. Alfano, "Biological materials probed by the temporal and angular profiles of the backscattered ultrafast laser pulses," J. Opt. Soc. Am. B **7,** 1685–1693 (1990).
14. R. R. Anderson and J. A. Parrish, *The Science of Photomedicine,* J. D. Regan and J. A. Parrish, eds. (Plenum, New York, 1982), Chap. 6, p. 147.
15. K. M. Case and P. F. Zweifel, *Linear Transport Theory* (Addison-Wesley, Reading, Mass., 1967).
16. H. S. Carslaw, "Some multiform solutions of the partial differential equations of physical mathematics and their applications," Proc. London Math. Soc. **30,** 121–161 (1898).
17. A. Sommerfeld, "Über verzweigte Potentiale im Raum," Proc. London Math. Soc. **28,** 395–429 (1897); **30,** 161–163 (1898).
18. J. H. Jeans, *Mathematical Theory of Electricity and Magnetism* (Cambridge U. Press, London, 1933).
19. B. A. Feddersen, D. W. Piston, and E. Gratton, "Digital parallel acquisition in frequency domain fluorometry," Rev. Sci. Instrum. **60,** 2929–2936 (1989).
20. B. Barbieri, F. De Picoli, M. vandeVen, and E. Gratton, "What determines the uncertainty of phase and modulation measurements in frequency domain fluorometry?" in *Time-Resolved Laser Spectroscopy in Biochemistry II,* J. R. Lakowicz, ed., Proc. Soc. Photo-Opt. Instrum. Eng. **1204,** 158–170 (1990).